# 1,500 year quantitative reconstruction of winter precipitation in the Pacific Northwest

Byron A. Steinman[a,1,2], Mark B. Abbott[a], Michael E. Mann[b], Nathan D. Stansell[c], and Bruce P. Finney[d]

[a]Department of Geology and Planetary Science, University of Pittsburgh, 4107 O'Hara Street, SRCC Room 200, Pittsburgh, PA 15260-3332; [b]Department of Meteorology and Earth and Environmental Systems Institute, Pennsylvania State University, 503 Walker Building, University Park, PA 16802-5013; [c]Byrd Polar Research Center, Ohio State University, 1090 Carmack Road, Scott Hall Room 108, Columbus, OH 43210-1002; and [d]Geosciences and Biological Sciences, Idaho State University, 921 South 8th Avenue, Stop 8072, Pocatello, ID 83209-8072

Edited by Mark H. Thiemens, University of California San Diego, La Jolla, CA, and approved May 28, 2012 (received for review January 20, 2012)

**Multiple paleoclimate proxies are required for robust assessment of past hydroclimatic conditions. Currently, estimates of drought variability over the past several thousand years are based largely on tree-ring records. We produced a 1,500-y record of winter precipitation in the Pacific Northwest using a physical model-based analysis of lake sediment oxygen isotope data. Our results indicate that during the Medieval Climate Anomaly (MCA) (900–1300 AD) the Pacific Northwest experienced exceptional wetness in winter and that during the Little Ice Age (LIA) (1450–1850 AD) conditions were drier, contrasting with hydroclimatic anomalies in the desert Southwest and consistent with climate dynamics related to the El Niño Southern Oscillation (ENSO) and the Pacific Decadal Oscillation (PDO). These findings are somewhat discordant with drought records from tree rings, suggesting that differences in seasonal sensitivity between the two proxies allow a more compete understanding of the climate system and likely explain disparities in inferred climate trends over centennial timescales.**

lake modeling | oxygen isotopes | American West

Water resources in the American west are under increasing stress because of growing demand and reduced availability caused by recent drought conditions (1). Developing temporal and spatial records of the timing, frequency, and magnitude of drought and its relationship with larger-scale climate patterns should help improve predictions of climate responses to projected future warming (2). Inconsistency among various paleoaridity proxies, however, is an obstacle to investigations of the connections between long-term, large-scale climate dynamics and regional drought. Here we examine past relationships between Pacific Ocean dynamics and winter precipitation in the Pacific Northwest through a model-based analysis of sediment oxygen isotope ($\delta^{18}$O) values from Castor Lake (3–5) and Lime Lake, Washington (Fig. 1). We compare our results to regional tree-ring data and other lake sediment $\delta^{18}$O records to assess geographic wet/dry patterns in western North America.

## Study Site.

Castor Lake and Lime Lake are located east of the Cascade Range in the relatively dry PDO/ENSO sensitive region of eastern Washington (Fig. 1). Both lakes are of late Wisconsinin glacial origin with small surface areas (<0.1 km$^2$) and maximum depths of approximately 12 m and 15 m, respectively. The Castor Lake (48.54 °N, 119.56 °W, elevation 594 m) catchment is located on a plateau several hundred meters above the Okanogan River valley and is isolated from distal groundwater sources. Modeling and observational studies demonstrate that evaporation is the primary water loss pathway and that input to the lake is limited to precipitation and catchment derived groundwater (4). Lime Lake is located in northeastern Washington (48.87 N, 117.34 W, elevation 780 m) in the Selkirk Mountains. The lake catchment is positioned well above regional groundwater on the eastern flank of the Pend Oreille River Valley. Surficial outflow occurs on a permanent basis from the southern shoreline. The lake catchment area is large producing substantial runoff and groundwater throughflow. Measurements of lake and local meteoric water $\delta^{18}$O values obtained over a six-year period (2005–2011 AD) demonstrate that Lime Lake water is relatively unaffected (isotopically) by evaporation (see *SI Appendix*, Fig. S1).

Precipitation in the Pacific Northwest is largely controlled by the strength and position of the Aleutian Low and North Pacific high-pressure systems and the associated westerly winds that deliver wet air to the continental interior in winter (6). Dry years typically occur when the Aleutian Low intensifies and promotes a stronger meridional component to the North Pacific westerlies and vice versa. ENSO and the PDO influence precipitation amounts in the western United States by modifying the strength and position of the Aleutian Low and North Pacific high-pressure systems.

## Results and Discussion

Lake sediment $\delta^{18}$O records have considerable potential as recorders of multidecadal to century-scale climate change because they can be quantitatively interpreted using physically-based models. In the small basins discussed here, the physical processes that control lake-catchment hydrology and isotope dynamics on decadal timescales also control lake dynamics on century-long timescales (4, 5) suggesting that well designed models should describe decade- and century-scale lake processes with similar accuracy.

Castor Lake water and sediment oxygen isotope values are primarily influenced by catchment water balance variations resulting from precipitation-evaporation forcing (4). Lime Lake $\delta^{18}$O values, however, are controlled by the isotopic composition of meteoric water (i.e., rain and snowfall), which is influenced by the origin of atmospheric moisture, air mass trajectory, Rayleigh distillation, and air temperature (7). Variations in meteoric water $\delta^{18}$O establish a baseline for Castor Lake water $\delta^{18}$O responses to hydrologic (rather than isotopic) processes such as evaporation from the lake surface and inflow from the catchment.

To establish a meteoric water baseline for the Castor Lake record, we mean centered the independently dated (*SI Appendix*, Table S1) Lime Lake $\delta^{18}$O data and subtracted these variations from the mean centered Castor Lake $\delta^{18}$O values (Figs. 2 and 3) thereby isolating the isotopic influence of hydrologic forcing on the Castor lake-catchment system (8). The resulting $\Delta\delta^{18}$O record represents the cumulative isotopic effects of evaporation

Author contributions: B.A.S., M.B.A., and B.P.F. designed research; B.A.S., M.B.A., and N.D.S. performed research; B.A.S. contributed new reagents/analytic tools; B.A.S., M.B.A., M.E.M., N.D.S., and B.P.F. analyzed data; and B.A.S., M.B.A., and M.E.M. wrote the paper.

The authors declare no conflict of interest.

This article is a PNAS Direct Submission.

Data deposition: Precipitation reconstruction data are available for download at the NCDC/NOAA Paleoclimate data archive website (www.ncdc.noaa.gov/paleo).

[1]Present address: Department of Meteorology and Earth and Environmental Systems Institute, Pennsylvania State University, 528 Walker Building, University Park, PA 16802-5013.

[2]To whom correspondence should be addressed. E-mail: bas56@psu.edu.

This article contains supporting information online at www.pnas.org/lookup/suppl/doi:10.1073/pnas.1201083109/-/DCSupplemental.

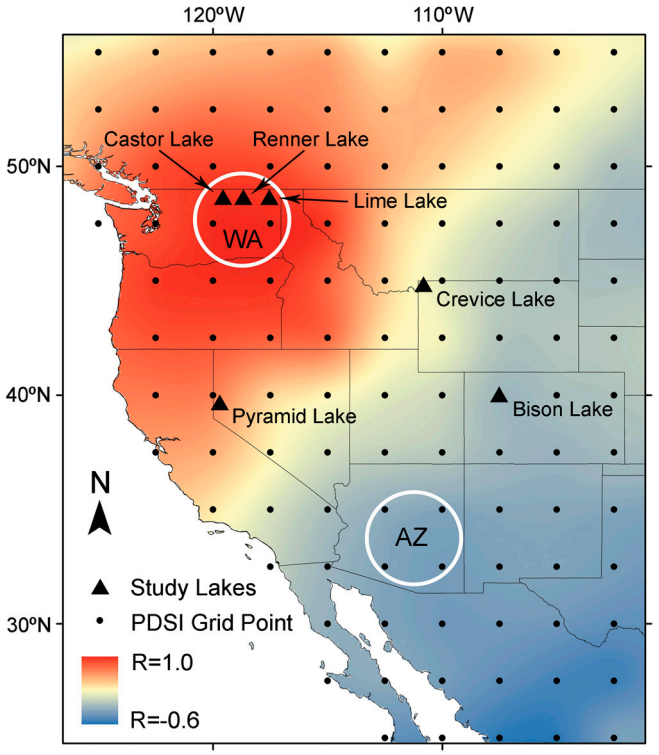


**Fig. 1.** Tree-ring based PDSI reconstruction correlation map for the western United States developed using data from Cook et al. (28). Correlations between data for eastern Washington (i.e., the average of grid points 43 and 55) and all other individual grid points were calculated using 20-year moving averages from the common time period (1645–2003 AD). Results were contoured using interpolation to improve visualization.

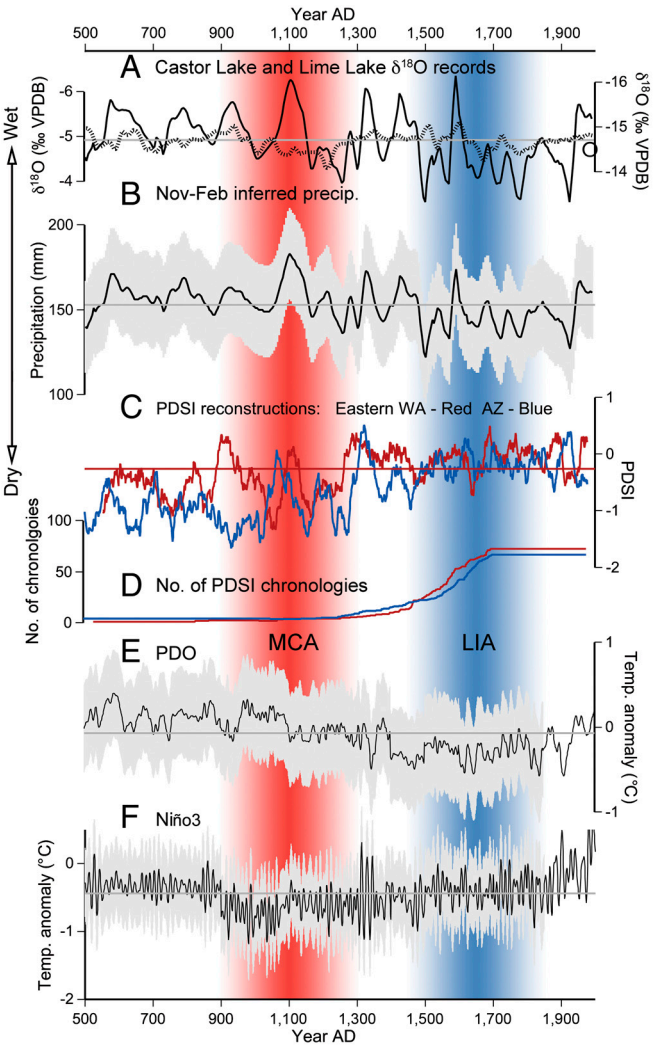


**Fig. 2.** (*A*) Castor Lake (solid line) and Lime Lake (dashed line) sediment $\delta^{18}O$ records. Twenty-year moving averages of Castor Lake values are displayed on the *y*-axis with limits of −4 and −6‰. Theoretical modern calcite values for Lime Lake were calculated using interpolated precipitation $\delta^{18}O$ values (open circle) (see *SI Appendix*). Note that *y*-axes are reversed for consistency. (*B*) Twenty-year average November—February precipitation for eastern Washington reconstructed using the Castor-Lime Lake $\Delta\delta^{18}O$ record (Fig. 3) and lake-catchment mass balance modeling. (*C*) PDSI reconstructions (28) from grid points 43 and 55 (average values for eastern Washington shown in red) and 88, 89, 104, and 105 (average values for Arizona shown in blue). Fifty year moving averages are displayed. (*D*) The number of chronologies used in the PDSI reconstructions for eastern Washington (red) and Arizona (blue). (*E*) PDO and (*F*) Niño3 reconstructions of Mann et al. (21). The PDO reconstruction is based on the SST averaged over the central North Pacific region 22.5 °N–57.5 °N and 152.5 °E–132.5 °W. The Niño3 region is 2.5 °S–2.5 °N and 92.5 °W–147 °W.

and water input/output (runoff and groundwater) to Castor Lake and does not represent changes in the isotopic composition of meteoric water. More positive $\Delta\delta^{18}O$ values indicate a relative deficit of catchment water and drier conditions, whereas more negative $\Delta\delta^{18}O$ values indicate a surplus of catchment water and wetter conditions.

To produce the 1,500 y precipitation reconstruction, we conducted an ensemble of Monte Carlo simulations using a combined lake-catchment, hydrologic, and isotope mass balance model that simulated Castor Lake isotopic evolution over discrete 20 y periods in response to randomly generated changes in monthly precipitation, temperature, and relative humidity (see *Materials and Methods*). Results indicate that November—February rain/snowfall is the strongest control on Castor Lake sediment $\delta^{18}O$ values and modeled $\Delta\delta^{18}O$ values (*SI Appendix*, Figs. S2–S4). We applied model-derived associations between 20-y average November—February precipitation and $\Delta\delta^{18}O$ anomalies to produce estimates for past precipitation amounts within statistically derived prediction limits (*SI Appendix*, Fig. S5). Observed 20th century precipitation amounts strongly correlate ($R^2 = 0.65$) to model reconstructed values (Fig. 4 and *SI Appendix*, Fig. S6).

Observational and modeling studies have established dynamical and statistical links between ENSO and midlatitude variability of the PDO (9–12) that paleorecords have confirmed (13). The teleconnections linking ENSO and the PDO, known as the "atmospheric bridge" (9), produce an association between El Niño events and warm PDO phases, and vice versa (10–12). Comparison of the Castor-Lime Lake precipitation record with tree-ring based PDO reconstructions (14–17) from western North America demonstrates that more (less) precipitation occurs in eastern Washington during "cool" ("warm") PDO phases (Fig. 5). The generally small decadal-scale disparities between individual PDO reconstructions and the lake sediment data are likely caused by a combination of the intrinsic uncertainties in the reconstructions, inconsistency in regional expressions of the PDO, and factors other than the PDO that impact hydroclimate in the Pacific Northwest (18–20).

Comparison of the Castor-Lime Lake precipitation record with the Mann et al. (21) PDO series reveals a strong centennial timescale relationship over the past 1,500 y between winter precipitation amounts in eastern Washington and PDO temperature anomalies (Fig. 2). During and prior to the MCA, for example, the north Pacific Ocean was generally warmer and winter precipitation amounts in Washington correspondingly greater than during the LIA when the opposite pattern occurred. A similar (although less consistent) centennial relationship exists between

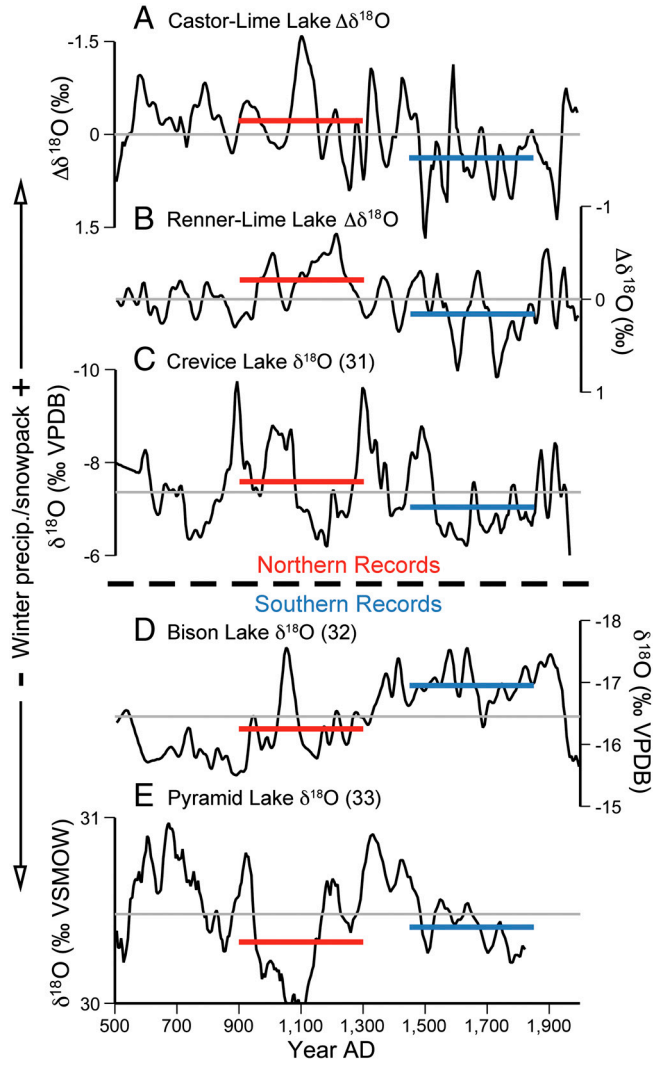


**Fig. 3.** (*A*) Castor-Lime Lake $\Delta\delta^{18}O$ record calculated by mean centering the Lime Lake and Castor Lake $\delta^{18}O$ records and subtracting the former from the latter. (*B*) Renner-Lime Lake $\Delta\delta^{18}O$ record developed using methods applied to the Castor-Lime Lake $\Delta\delta^{18}O$ record (see *SI Appendix*). (*C*) Crevice Lake $\delta^{18}O$ record (31). (*D*) Bison Lake $\delta^{18}O$ record (32). (*E*) Pyramid Lake $\delta^{18}O$ record (33). The northern records indicate that winter precipitation/snowpack amounts were greater in the Pacific Northwest during the MCA and that during the LIA drier winter conditions prevailed. The southern records indicate the opposite, i.e., that winters during the LIA were wetter relative to the MCA.

reconstructed Niño3 values and winter rain/snowfall in which higher Niño3 temperatures are associated with smaller precipitation amounts and vice versa. The exceptionally high precipitation levels in the Pacific Northwest during the MCA could have resulted from a combination of warmer north Pacific sea surface temperatures and La Niña-like conditions in the tropical Pacific. Our interpretation of the MCA as being characterized by La Niña-like mean state conditions is corroborated by other paleoproxy studies (22–24) as well as climate model simulations (25) further suggesting that observed (18, 26, 27) interannual to decadal relationships between ENSO, PDO, and winter precipitation amounts in the Pacific Northwest are represented by similar anomalies on century-long timescales.

The drought reconstructions of Cook et al. (28) appear to be at odds with our results from the Pacific Northwest. Although the Castor-Lime Lake winter precipitation record and the regional Palmer Drought Severity Index (PDSI) records (28) (grid points 43 and 55) are well (anti)correlated on multidecadal timescales

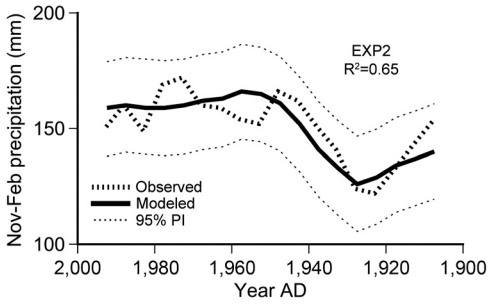


**Fig. 4.** Comparison between 20-year average modeled and observed 20th century precipitation amounts. Three similar reconstructions (*SI Appendix*, Fig. S6) resulting from the application of different outseepage configurations were produced (see *SI Appendix*).

(3), they do not exhibit consistent long-term trends (Fig. 2). The tree-ring data, for example, suggest that conditions were relatively drier in the Pacific Northwest during the MCA, whereas the Castor Lake record suggests that winters were wetter. Notably, the Cook et al. (28) data also point to a dry MCA in the desert southwest, contrasting with the antiphasing between the multidecadal responses in the northwest and southwest over the past approximately 350 y in the PDSI reconstructions (Fig. 1).

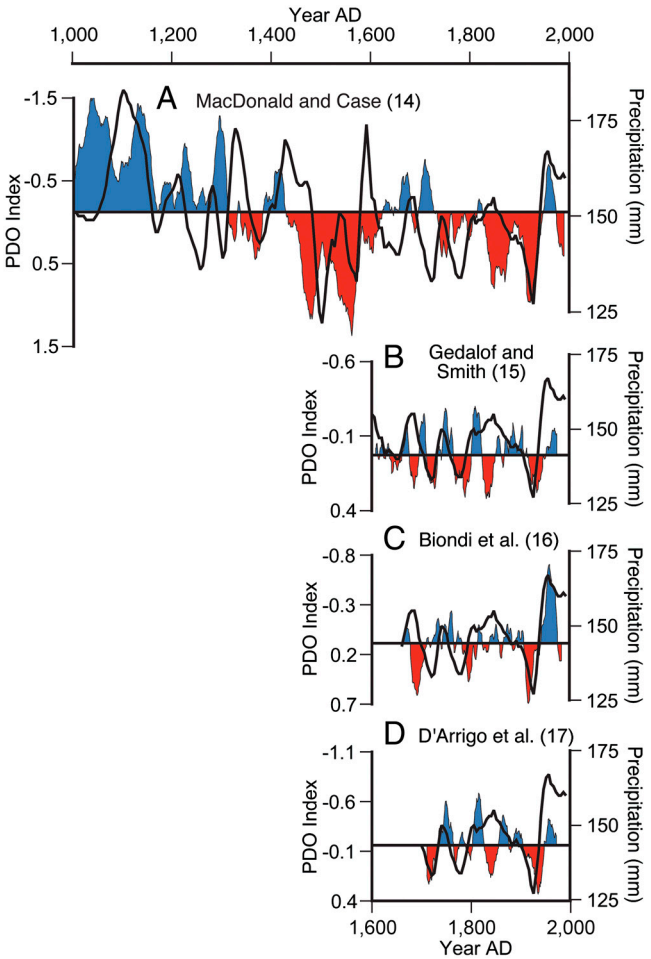


**Fig. 5.** Castor Lime-Lake precipitation record (black line) compared to the (*A*) MacDonald and Case (14), (*B*) Gedalof and Smith (15), (*C*) Biondi et al. (16), and D'Arrigo et al. (17) tree-ring based PDO reconstructions. The average value of each PDO dataset is depicted by the line separating the red (warm) and blue (cool) PDO phases. *Y*-axes are not identically scaled to improve visualization. Twenty-year moving averages of data are displayed.

Differences in the seasonal sensitivities of the tree-ring based PDSI and lake sediment oxygen isotope data may in part explain the apparent discrepancies between the two proxies. For example, Castor-Lime Lake $\Delta\delta^{18}O$ values are primarily controlled by variability in catchment runoff resulting from precipitation during colder seasons (i.e., late fall through early spring) when evapotranspiration rates are low. Conversely, growth rates in drought sensitive trees are primarily controlled by soil moisture content during the growing season (i.e., spring and summer) and are used to reconstruct summer PDSI values that incorporate temperature and precipitation (but not snowpack and melt) data from an approximately 12 mo period (29). One scenario that could explain the differences during the MCA is that winters were generally wetter, which shifted the Castor-Lime Lake $\Delta\delta^{18}O$ baseline toward more negative values, but that summers and possibly springs were hotter and drier, which produced inferred drought conditions in the tree-ring records. It is, therefore, likely that (rather than being in direct contrast) the lake sediment oxygen isotope data and the tree-ring based PDSI records consistently exhibit distinct seasonal responses to climate resulting from the disparate physical and biological processes that control the responses of lakes and trees to hydroclimatic change. The relatively limited number of older chronologies (Fig. 2) combined with the large uncertainty in low frequency variance derived from Regional Curve Standardization (RCS) methods of tree ring data analysis (30) could also contribute to differences between the two paleoclimate archives.

Oxygen isotope records from Renner Lake, Washington (48.78 °N, 118.19 °W, elevation 754 m) (see *SI Appendix*) and Crevice Lake, Wyoming (45.00 °N, 110.58 °W, elevation 1,713 m) (31) provide support for the Castor-Lime Lake precipitation reconstruction indicating that winter conditions during the MCA and LIA were relatively wetter and drier, respectively (Fig. 3). Notably, an oxygen isotope record from Bison Lake, Colorado (39.76 °N, 107.35 °W, elevation 3,255 m) (32) demonstrates the opposite pattern, that is, drier winters during the MCA and wetter winters during the LIA, a scenario generally supported by oxygen isotope data (and other proxy evidence) from Pyramid Lake, Nevada (40.00 °N, 119.55 °W, elevation 1,159 m) (33) and other Great Basin lakes (34). Combined, these records indicate that a north-south antiphasing pattern of winter drought (similar to the multidecadal pattern diagnosed from the tree-ring PDSI data) occurred over the past 1,500 y on century-long time scales with an "axis" between the north and south that likely fell between northern Oregon and California and extended eastward into northwestern Wyoming.

The strong association between winter precipitation in the western United States, ENSO and the PDO, as well as similarities to other regional records, indicates that the Castor-Lime Lake precipitation record is a reliable indicator of past variability in Pacific Ocean surface temperatures on decade- to century-long timescales. In contrast, tree-ring based PDSI reconstructions may be more strongly influenced by temperature and rain/snowfall in seasons (i.e., summer and spring) that are not as heavily affected by ENSO and the PDO (which have a greater effect on climate in winter). The century-scale coherence between the Mann et al. (21) PDO record and the Castor-Lime Lake $\Delta\delta^{18}O$ record during the MCA and LIA supports this assertion and further indicates that multiple proxies with different seasonal sensitivities (e.g., lakes and trees) are required for a more comprehensive understanding of the climate system. The Castor-Lime Lake winter precipitation record suggests that the "great droughts" indicated by tree rings for the American West during the MCA either did not include much of the Pacific Northwest or did not occur in winter and that a north-south, contrasting pattern of precipitation trends similar to that observed during the 20th century (18, 26, 27) prevailed on centennial timescales over the last 1,500 y.

## Materials and Methods

**Castor Lake Sediment Core Recovery and Sampling.** The Castor Lake age model and sediment core collection and sampling methods are described by Nelson et al. (3).

**Lime Lake Sediment Core Recovery and Sampling.** In October 2006, we collected sediment cores from Lime Lake using a modified Livingstone corer and a piston corer designed to retrieve undisturbed sediment-water interface profiles. Surface sediments were extruded in the field at 0.5 cm intervals by upward extrusion into a sampling tray fitted to the top of the core barrel. At the University of Pittsburgh, cores were sampled at approximately 1–5 mm intervals for carbonate mineral stable isotope analysis. Sediment samples were disaggregated for approximately 24 h in 7% $H_2O_2$ solution and sieved at 63 μm to isolate authigenic (i.e., precipitated in-lake) carbonate material and to limit contamination by biogenic carbonate shell material. The captured <63 μm fraction of the sediment was settled from rinse water and then centrifuged, and the remaining liquid was decanted. The resulting fine-grained carbonate sediment was bleached (using a 50% bleach, 50% water solution), rinsed three times using deionized water, freeze-dried, and homogenized using an agate mortar and pestle. Isotopic ratios were measured at the University of Arizona Environmental Isotope Laboratory using an automated carbonate preparation device (KIEL-III) coupled to a gas-ratio mass spectrometer (Finnigan MAT 252). Powdered samples were reacted with dehydrated phosphoric acid under vacuum at 70 °C. Isotopic values are expressed in conventional delta ($\delta$) notation as the per mil (‰) deviation from Vienna PeeDee Belemnite (VPDB). Analytical precision (based on repeated measurements of NBS-18 and NBS-19 carbonate standard materials) was better than 0.1‰. A description of the Lime Lake $\delta^{18}O$ record and age model are provided in the *SI Appendix*.

Sediment characterization by X-ray diffractometry was completed at the University of Pittsburgh's Materials Micro-Characterization Laboratory using a Phillips X'Pert Powder Diffractometer over a $2\theta$ range of 10–80°. X-ray diffraction results indicate that calcite is the only detectable mineral in the fine-grained, carbonate sediment at Lime Lake.

**Monte Carlo Simulations.** To quantitatively interpret the combined, Castor Lake and Lime Lake $\Delta\delta^{18}O$ record, we conducted a suite of Monte Carlo simulations in which we forced the modified Steinman et al. (4) model (see *SI Appendix*) using white noise (with even and normal distributions) applied to monthly climate variables, namely precipitation, temperature and relative humidity (RH) (*SI Appendix*, Figs. S7–S9). Prior to each simulation, randomly selected average values for each climate variable for each calendar month were determined (within the model) using an even distribution random number algorithm. Climate variable input limits (i.e., the domain of the Monte Carlo simulations) were based on analyses of decadal variations in instrumental data (*SI Appendix*, Table S2). Experiments were conducted in which monthly temperature and precipitation were altered within a range defined by the average value for the 20th century and the largest observed deviation (of the 20 y average) from this value. For example, the model selected an average precipitation amount of $46 \pm 16$ mm for December at the beginning of each test that established the mean values for this month in all following simulation years. Stochastic variance was then imparted (within the model) to these monthly mean values using a randomly generated, log normal distribution (developed using the interannual standard deviation for each month over the instrumental period) to produce random, interannual variance in monthly precipitation. Likewise, the model generated average monthly temperatures within a range defined by observed 20 y average temperature changes and then imparted stochastic variance (using a normal distribution) to these mean monthly values over the course of the simulation. RH values were defined as a function of temperature and then randomly varied (using an even distribution) within the 95% prediction confidence intervals of an RH-temperature regression relationship developed using instrumental weather data. Comparison of monthly temperature and precipitation data demonstrates that no significant relationship exists between the two variables (i.e., they are unrelated on a monthly time scale). For example, linear regression equations relating year to year (e.g., January observations over the instrumental period) monthly precipitation totals (predictor) to average temperature (predictand) have an average correlation ($R^2$) value of 0.05.

**Precipitation Reconstruction.** We conducted one hundred simulations (in each exponential outseepage configuration) on a monthly time step over 40 y of which the first 20 were a model equilibration period. Sediment $\delta^{18}O$ and $\Delta\delta^{18}O$ values for each year in the model simulations were produced by averaging the May—July model predicted $\delta^{18}O$ values (see *SI Appendix*,

Figs. S10–S12). For each simulation, the final 20 annual sediment $\delta^{18}O$ and $\Delta\delta^{18}O$ values were averaged (i.e., a 20 y average was produced for $\delta^{18}O$ and $\Delta\delta^{18}O$ values) and related to climate variable averages over the common time period. Specifically, these 20 y average modeled sediment $\delta^{18}O$ and $\Delta\delta^{18}O$ values were compared to November—February, March—June, and July—October average precipitation, temperature, and relative humidity (*SI Appendix*, Figs. S2–S4). November—February precipitation exhibited a stronger correlation to modeled $\Delta\delta^{18}O$ values than did average temperature and relative humidity in all seasons (with $R^2$ values as high as 0.82). In addition, the range of measured Castor Lake $\delta^{18}O$ values (approximately −3.5 to −6.5‰) and Castor-Lime Lake $\Delta\delta^{18}O$ anomalies (approximately ±1.5‰) were reproduced in model experiments. We selected 20 y averages for analysis in order to strike a balance between achieving a high enough temporal resolution for model validation (through comparison to 20th century observations) and minimizing uncertainty errors introduced by unknown initial conditions (i.e., the hydrologic and isotopic state of the lake-catchment system at the beginning of the period of analysis).

We used linear regression to analyze the relationship between the simulated 20 y average November—February precipitation and sediment $\Delta\delta^{18}O$ values (*SI Appendix*, Fig. S5). Prediction limits (at the 95% level) were calculated for the precipitation-sediment $\Delta\delta^{18}O$ relationships in order to constrain uncertainty in the reconstructions. The linear regression equation was applied to the Castor-Lime Lake sediment $\Delta\delta^{18}O$ record to reproduce corresponding 20 y average precipitation amounts (Fig. 2).

Twenty-year average modeled November—February precipitation amounts for the instrumental period (1900–2007 AD) strongly correlate to observational data with an $R^2$ value of 0.65 in all three exponential outseepage scenarios (Fig. 4, *SI Appendix*, Fig. S6). In each case observed precipitation values fall within modeled prediction limits demonstrating that changes to the exponential decay function (within the ranges presented here) do not strongly influence model results. To produce the 1,500 y November—February precipitation reconstruction, we averaged results from the three Monte Carlo scenarios and applied the prediction limits with the largest range (i.e., those from the EXP3 scenario).

Model reconstructed November—February precipitation amounts varied (over the past 1,500 y) between 184 and 119 mm, 182 and 121 mm, and 182 and 126 mm in the EXP1, EXP2, and EXP3 scenarios, respectively, with prediction limits (at the 95% level) of ±19, 21, and 27 mm. Values obtained by averaging all three scenarios varied between 183 and 122 mm.

**ACKNOWLEDGMENTS.** We thank Chris Helander, Jeremy Moberg, and Daniel Nelson. This work was funded by the Paleo Perspectives on Climate Change and the Atmospheric Sciences programs of the National Science Foundation.

1. Cook ER, Seager R, Cane MA, Stahle DW (2007) North American drought: Reconstructions, causes, and consequences. *Earth-Sci Rev* 81:93–134.
2. Goosse H, et al. (2010) Reconstructing surface temperature changes over the past 600 years using climate model simulations with data assimilation. *J Geophys Res* 115:D09108.
3. Nelson DB, et al. (2011) A 6,000 year lake record of drought from the Pacific Northwest. *Proc Natl Acad Sci USA* 108:3870–3875.
4. Steinman BA, Rosenmeier MF, Abbott MB, Bain DJ (2010a) The isotopic and hydrologic response of small, closed-basin lakes to climate forcing from predictive models: Application to paleoclimate studies in the upper Columbia River basin. *Limnol Oceanogr* 55:2231–2245.
5. Steinman BA, Rosenmeier MF, Abbott MB (2010b) The isotopic and hydrologic response of small, closed-basin lakes to climate forcing from predictive models: Simulations of stochastic and mean state precipitation variations. *Limnol Oceanogr* 55:2246–2261.
6. Bryson RA, Hare KF, eds. (1974) *World Survey of Climatology* (Elsevier, New York), chap. 1.
7. Rozanski K, Araguás-Araguás L, Gonfiantini R (1993) *Climate Change in Continental Isotopic Records*, eds PH Swart, KC Lohmann, J McKenzie, and S Savin (American Geophysical Union, Washington), chap. 1.
8. Anderson L, Abbott MB, Finney BP, Burns SJ (2007) Late Holocene moisture balance variability in the southwest Yukon Territory, Canada. *Quat Sci Rev* 26:130–140.
9. Alexander MA, et al. (2002) The atmospheric bridge: The influence of ENSO teleconnections on air-sea interaction over the global oceans. *J Climate* 15:2205–2231.
10. Newman M, Compo GP, Alexander MA (2003) ENSO-forced variability of the Pacific decadal oscillation. *J Climate* 16:3853–3857.
11. Vimont D (2005) The contribution of the interannual ENSO cycle to the spatial pattern of decadal ENSO-like variability. *J Climate* 18:2080–2092.
12. Di Lorenzo E, et al. (2010) Central Pacific El Niño and decadal climate change in the North Pacific Ocean. *Nat Geosci* 3:762–765.
13. Verdon DC, Franks SW (2006) Long-term behavior of ENSO: Interactions with the PDO over the past 400 years inferred from paleoclimate records. *Geophys Res Lett* 33:L06712.
14. MacDonald GM, Case RA (2005) Variations in the Pacific Decadal Oscillation over the past millennium. *Geophys Res Lett* 32:L08703.
15. Gedalof Z, Smith DJ (2001) Interdecadal climate variability and regime-scale shifts in Pacific North America. *Geophys Res Lett* 28:1515–1518.
16. Biondi F, Gershunov A, Cayan DR (2001) North Pacific decadal climate variability since AD 1661. *J Climate* 14:5–10.
17. D'Arrigo R, Villalba R, Wiles G (2001) Tree-ring estimates of Pacific decadal climate variability. *Clim Dynam* 18:219–224.
18. Wise EK (2010) Spatiotemporal variability of the precipitation dipole transition zone in the western United States. *Geophys Res Lett* 37:L07706.
19. McCabe GJ, Palecki MA, Betancourt JL (2004) Pacific and Atlantic Ocean influences on multidecadal drought frequency in the United States. *Proc Natl Acad Sci USA* 101:4136–4141.
20. Hidalgo HG (2004) Climate precursors of multidecadal drought variability in the western United States. *Water Resour Res* 40:W12504.
21. Mann ME, et al. (2009) Global signatures and dynamical origins of the Little Ice Age and Medieval Climate Anomaly. *Science* 326:1256–1260.
22. Cobb KM, Charles CD, Cheng H, Edwards RL (2003) El Niño/Southern Oscillation and tropical Pacific climate during the last millennium. *Nature* 424:271–276.
23. Graham NE, et al. (2007) Tropical Pacific—Mid-latitude teleconnections in medieval times. *Clim Change* 83:241–285.
24. Trouet V, et al. (2009) Persistent positive North Atlantic Oscillation mode dominated the medieval climate anomaly. *Science* 324:78–80.
25. Mann ME, Cane MA, Zebiak SE, Clement A (2005) Volcanic and solar forcing of the tropical Pacific over the past 1,000 years. *J Climate* 18:447–456.
26. Cayan DR, Dettinger MD, Diaz HF, Graham NE (1998) Decadal variability of precipitation over western North America. *J Climate* 11:3148–3166.
27. Dettinger MD, Cayan DR, Diaz HF, Meko DM (1998) North-south precipitation patterns in western North America on interannual-to-decadal timescales. *J Climate* 11:3095–3111.
28. Cook ER, Woodhouse CA, Meko DM, Stahle DW (2004) Long-term aridity changes in the western United States. *Science* 306:1015–1018.
29. Palmer WC (1965) *Meteorological Drought* (U.S. Department of Commerces, Washington, DC), Weather Bureau Research Paper 45.
30. Jones PD, et al. (2009) High-resolution palaeoclimatology of the last millennium: A review of current status and future prospects. *Holocene* 19:3–49.
31. Stevens LR, Dean WE (2008) Geochemical evidence for hydroclimatic variability over the last 2,460 years from Crevice Lake in Yellowstone National Park, USA. *Quat Int* 188:139–148.
32. Anderson L (2011) Holocene record of precipitation seasonality from lake calcite $\delta^{18}O$ in the central Rocky Mountains, United States. *Geology* 39:211–214.
33. Benson L, et al. (2002) Holocene multidecadal and multicentennial droughts affecting Northern California and Nevada. *Quat Sci Rev* 21:659–682.
34. Kleppe JA, et al. (2011) Duration and severity of Medieval drought in the Lake Tahoe Basin. *Quat Sci Rev* 30:3269–3279.